Coexistence of bound soliton and harmonic mode-locking soliton in an ultrafast fiber laser based on MoS_2-deposited microfiber photonic device

Meng Liu (刘 萌)[1,2], Aiping Luo (罗爱平)[1,2], Wencheng Xu (徐文成)[1,2], and Zhichao Luo (罗智超)[1,2,*]

[1]*Guangdong Provincial Key Laboratory of Nanophotonic Functional Materials and Devices & Guangzhou Key Laboratory for Special Fiber Photonic Devices and Applications, South China Normal University, Guangzhou 510006, China*

[2]*Guangdong Provincial Engineering Technology Research Center for Microstructured Functional Fibers and Devices, South China Normal University, Guangzhou 510006, China*

**Corresponding author: zcluo@scnu.edu.cn*

Received October 30, 2017; accepted December 22, 2017; posted online January 26, 2018

As the typical material of two-dimensional transition metal dichalcogenides (TMDs), few-layered MoS_2 possesses broadband saturable absorption and a large nonlinear refractive index, which could be regarded as a promising candidate for dual-function photonic device fabrication. In this work, the coexistence of a bound soliton and harmonic mode-locking soliton was demonstrated in an ultrafast fiber laser based on a MoS_2-deposited microfiber photonic device. Through a band-pass filter, each multi-soliton state was investigated separately. The bound soliton has periodic spectral modulation of 1.55 nm with a corresponding pulse separation of 5.16 ps. The harmonic mode-locking soliton has the repetition rate of 479 MHz, corresponding to the 65th harmonic of the fundamental repetition rate. The results indicated that there exist more possibilities of different multi-soliton composites, which would enhance our understanding of multi-soliton dynamics.

OCIS codes: 160.4330, 140.4050, 140.3510, 250.5530.
doi: 10.3788/COL201816.020008.

Two-dimensional (2D) materials have attracted much attention since the discovery of graphene in 2004. The 2D materials own many unique properties, such as wideband absorption, ultrafast carrier dynamics, and 2D planar advantage, which make the 2D materials play important roles in electronic and photonic applications[1–3]. Especially, graphene, the first of 2D materials, has been demonstrated to be an excellent saturable absorber (SA) in ultrafast fiber lasers because of its broadband saturable absorption and ultrafast nonlinear optical response[4–6]. However, the unique zero bandgap structure of graphene also brings intrinsic disadvantages, namely a degenerated light modulation ability[7], which would limit its potential applications in the related photonics fields requiring strong light–matter interaction. Inspired by the success of graphene, more efforts have been made to explore new types of 2D materials, such as topological insulator[8,9], black phosphorus[10,11], MXene[12], and bismuthene[13]. Recently, 2D semiconducting transition metal dichalcogenides (TMDs) have received significant attention because of their semiconducting properties with tunable bandgaps and abundance in nature[14–16]. MoS_2 is a typical TMD, which has layered-dependent electronic and optical properties[17,18]. In 2013, Wang *et al.* found that the few-layer MoS_2 exhibits a stronger saturable absorption response than graphene at a specific waveband[19]. Then, Zhang *et al.* demonstrated the broadband saturable absorption of few-layer MoS_2 at 400, 800, and 1060 nm wavebands by using both open-aperture Z scan and balanced-detector measurement techniques[20]. It indicated that the MoS_2 could be an excellent candidate for broadband SA fabrication. So far, the passive mode-locking or Q-switching has been achieved experimentally at different wavebands based on the MoS_2 SA[21–32]. Apart from the broadband saturable absorption, Wang *et al.* experimentally found that the MoS_2 also possesses a large nonlinear refractive index[33]. Then, it is expected that the MoS_2 could act as a promising material for dual-functional photonic devices with both saturable absorption and high nonlinear effect.

On the other hand, in addition to optical pulse sources, the passively mode-locked fiber lasers could also be regarded as great test beds for the investigation of soliton dynamics. As we know, when the nonlinear effects in the laser cavity are high enough, the single soliton will break up into multiple solitons, and then evolve into different types of multi-solitons through the interactions among solitons, dispersive waves, and continuous waves[34,35]. To date, various kinds of multi-soliton dynamics have been obtained in fiber lasers, such as harmonic mode-locking soliton[36–38], bound soliton[39,40], soliton rain[41,42], and noise-like soliton[43,44]. The investigations of multi-soliton phenomena would be meaningful to further understand the physical features of multi-solitons. Generally, the fiber laser would operate in one of the multi-soliton states with certain cavity conditions.

However, by precisely adjusting the cavity parameters, different types of multi-soliton states could also be generated simultaneously in the passively mode-locked fiber laser. Recently, Huang *et al.* reported the simultaneous generation of harmonic soliton molecules and rectangular noise-like pulses in a figure-eight fiber laser[45]. Then Wang *et al.* demonstrated the coexistence of a noise-like pulse and high repetition rate harmonic mode-locking in a dual-wavelength mode-locked Tm-doped fiber laser[46]. By filtering each multi-soliton state, these coexistences of disparate multi-soliton states could provide multiple pulse sources for different purposes, ranging from fundamental research to industrial applications. In addition, as mentioned above, the multi-soliton patterns could be frequently observed in a fiber laser with an SA and a highly nonlinear component, which could be provided by the few-layered MoS_2-based photonic device at the same time. In order to further enhance the nonlinear effect of MoS_2 photonic devices, we fabricated it by depositing the MoS_2 onto a microfiber, where the interaction length between light and MoS_2 is much longer than those obtained by other SA preparation methods[47,48]. It has been demonstrated that the MoS_2-deposited microfiber photonic devices could introduce strong nonlinear pulse shaping in the fiber laser for diverse multi-soliton formation[48]. Therefore, it is interesting to know whether some other multi-soliton coexistences could be achieved in the ultrafast fiber lasers based on the MoS_2-deposited microfiber photonic device.

In this work, the coexistence of bound soliton and harmonic mode-locking soliton was experimentally observed in an ultrafast fiber laser based on MoS_2-deposited microfiber photonic devices. By using a tunable band-pass filter, the two multi-soliton states were resolved. The spectrum of bound soliton is centered at 1559.17 nm with a modulation period of 1.55 nm. The harmonic mode-locking soliton has the typical spectrum of anomalous dispersion regime with a central wavelength of 1555.13 nm, and the repetition rate is 479 MHz, corresponding to the 65th harmonic of the fundamental repetition frequency. These experimental results further confirm that different multi-soliton operations could be coexistent in an ultrafast fiber laser and offer opportunities to investigate the bound soliton and harmonic mode-locking soliton simultaneously.

The MoS_2-deposited microfiber photonic device was fabricated by depositing the MoS_2 onto microfiber. The detailed process of fabrication of a MoS_2-deposited microfiber photonic device has been described in our previous work[48]. The diameter of microfiber used in this experiment is ~14 μm, and the deposition length of MoS_2 is ~1 mm. After accomplishing the process of deposition, the saturable absorption effect of the MoS_2-deposited microfiber photonic device was measured by using the power-dependent transmission technique. In this experiment, the non-saturable loss is ~46.4% and the modulation depth is ~1.77%. Its modulation depth is low and its non-saturable loss is a little high. However, the quality of the MoS_2-deposited microfiber photonic device could be further improved by optimizing the deposition length of MoS_2 and the diameter of microfiber. In addition, the MoS_2-deposited microfiber photonic device has good long term stability. Then, the prepared MoS_2-deposited microfiber photonic device was incorporated into the laser cavity. The schematic of the passively mode-locked erbium-doped fiber (EDF) laser with MoS_2-deposited microfiber is shown in Fig. 1. The total cavity length is ~27.7 m, including a segment of ~7 m EDF and ~20.7 m single-mode fiber (SMF). So the fundamental repetition rate is calculated to be 7.37 MHz. Two polarization controllers (PCs) are employed to adjust the polarization state of the propagating light. A polarization-independent isolator (PI-ISO) is incorporated into the cavity in order to ensure the unidirectional operation of the fiber laser. The signal is coupled out from the cavity by a 10% optical coupler (OC). An optical spectrum analyzer (Anritsu MS9710C) and a real-time oscilloscope (Tektronix DSA 70804, 8 GHz) with a 12.5 GHz photodiode detector (New Focus P818-BB-35F) are used to monitor the laser performance. Moreover, the pulse profiles are measured by a commercial autocorrelator (FR-103XL).

By virtue of the saturable absorption of the MoS_2-deposited microfiber photonic device, the mode-locking operation could be easily realized in the proposed fiber laser. It should be noted that in our experiments, no passively *Q*-switching operation could be observed, which might be contributed to the low modulation depth of the proposed MoS_2-deposited microfiber. Due to the high nonlinear effect introduced by the MoS_2-deposited microfiber photonic device, the fiber laser always inclined to operate in the multi-soliton state, and, thus, the single-pulse energy would be limited to a relatively low level in this fiber laser. At the pump power of 65 mW, the harmonic mode-locking operation was achieved by adjusting the PC, as shown in Fig. 2. Figure 2(a) presents the spectrum of harmonic mode-locking operation, whose central wavelength and 3 dB bandwidth are 1556 and 1.49 nm, respectively. Here, we can clearly observe the Kelly sidebands on the mode-locked spectrum, which indicates that the fiber laser operates in the soliton regime with anomalous dispersion[49]. Figure 2(b) illustrates the mode-locked

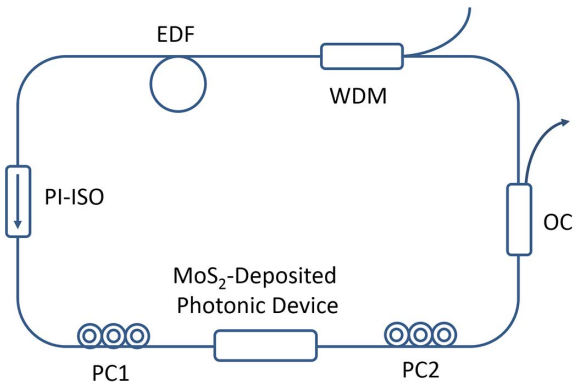

Fig. 1. Schematic of the passively mode-locked EDF laser with a MoS_2-deposited microfiber photonic device.

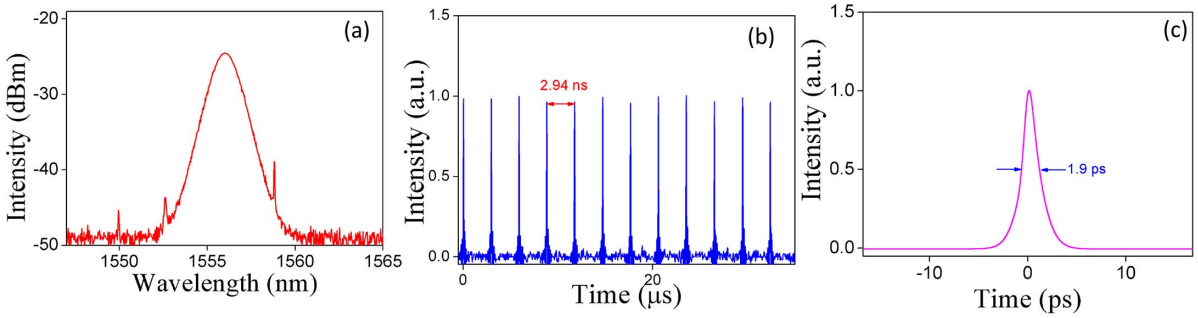

Fig. 2. Single-wavelength harmonic mode-locked operation at the repetition rate of 340 MHz. (a) Mode-locked spectrum; (b) corresponding pulse-train; (c) corresponding autocorrelation trace.

pulse-train with a repetition rate of 340 MHz, corresponding to the 46th harmonic of fundamental repetition frequency. By using the commercial autocorrelator, we measured the pulse duration to be 1.9 ps if a sech^2 shape pulse is assumed, as shown in Fig. 2(c).

As we know, together with the cavity birefringence, the polarization-dependent loss introduced by squeezing the fiber in PCs could produce the spectral filter, which could be used to generate the multi-wavelength operation in the fiber laser[50]. Therefore, by increasing the pump power to 78 mW and carefully adjusting the PC, the dual-wavelength multi-soliton states could be achieved in the fiber laser, as presented in Fig. 3. Figure 3(a) presents the spectrum of the dual-wavelength mode-locking operation. The spectrum at the shorter wavelength has obvious Kelly sidebands on the left side, and its central wavelength and 3 dB bandwidth are 1555.13 and 0.58 nm, respectively, while the spectrum at the longer wavelength locates at 1559.17 nm with the 3 dB bandwidth of 2.5 nm. Moreover, the spectral modulations with a period of 1.55 nm appear on the spectrum at a longer wavelength, which is one of the typical characteristics of bound soliton[32,33]. As shown in Fig. 3(b), the corresponding pulse-trains consist of two sequences of pulse-trains, which have different intensities and pulse separations. For better clarity, the pulse-train with a smaller scan range is also shown in the inset of Fig. 3(b). The sequence of the pulse-train with higher intensity is a kind of soliton bunch including 13 irregularly distributed pulses. The separation between soliton bunches is 135.6 ns, corresponding to the fundamental repetition rate of 7.37 MHz. The pulse-train with lower intensity has the repetition rate of 479 MHz, corresponding to the 65th harmonic of the fundamental repetition rate. Note that due to the different central wavelengths of the bound soliton and harmonic mode-locking soliton, the collision among them would happen frequently, and, then, they would recover their initial states after the collision. Figure 3(c) depicts the autocorrelation trace of the dual-wavelength mode-locked operation. There are three peaks with ~5.16 ps separation on the autocorrelation trace, which is believed to be a composite of the two multi-soliton states. In the experimental observation, the proposed fiber laser could sustain the dual-wavelength operation for a long time if there were no environment perturbations applied to the fiber laser.

It is expected that each sequence of the pulse-train is generated individually by the two wavelengths in different multi-soliton operation regimes. However, we could not identify the correspondence between the spectra and pulse-trains from the results presented in Fig. 3. Then, a band-pass filter was employed to resolve the lasing at each wavelength. Figure 4 provides the wavelength-resolved measurements. As shown in Figs. 4(a) and 4(b), the filtered spectra is centered at 1555.13 and 1559.17 nm, respectively. Figures 4(c) and 4(d) are the wavelength-resolved pulse-trains. The harmonic mode-locking soliton with a repetition rate of 479 MHz is at the shorter wavelength, while the soliton bunch corresponds to the longer wavelength of the bound soliton. In order to further confirm the two disparate multi-soliton operation regimes, the autocorrelation traces at each

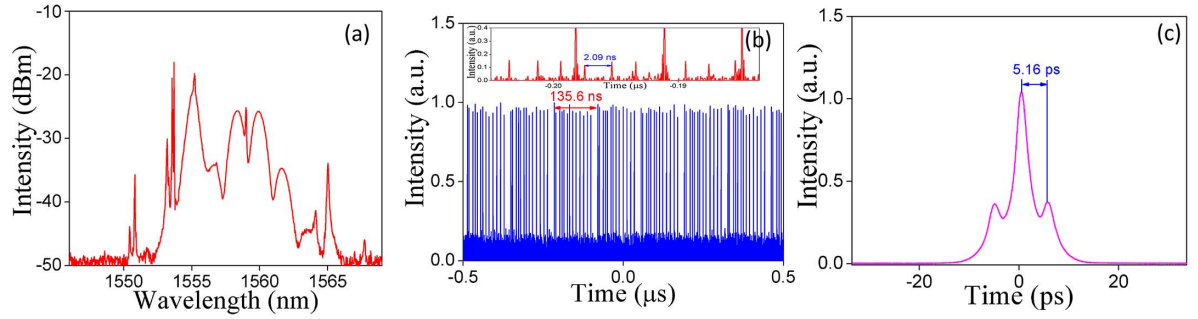

Fig. 3. Composite regime of bound soliton and harmonic mode-locking soliton. (a) Spectrum; (b) pulse-train; (c) autocorrelation trace.

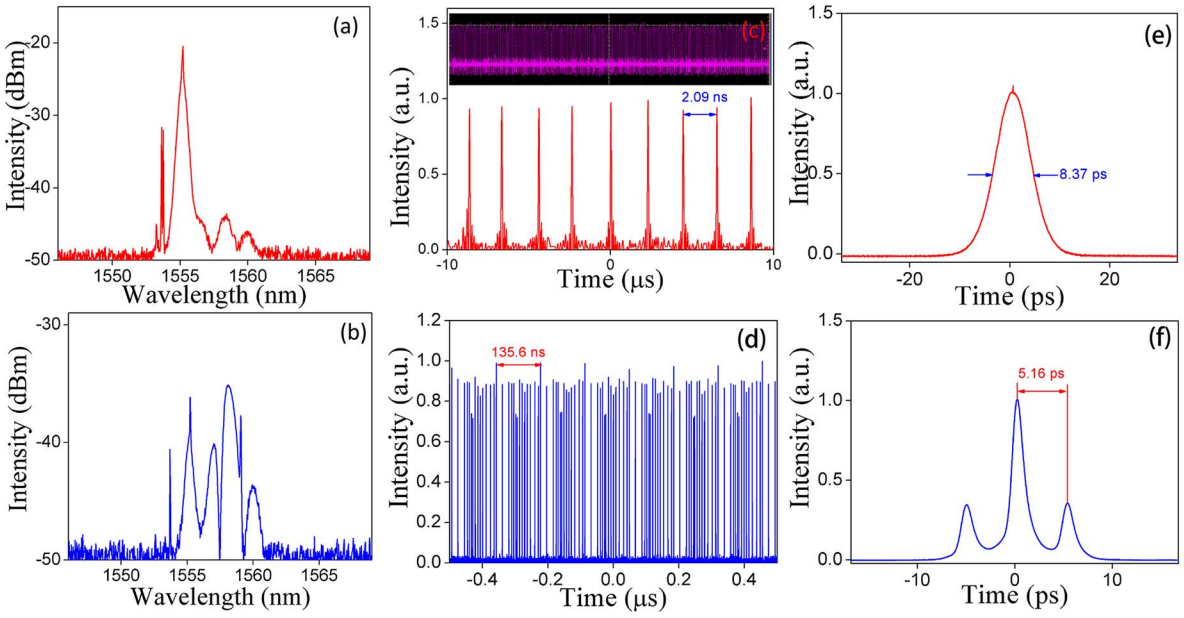

Fig. 4. Wavelength-resolved operation. (a), (b) Spectra centered at 1555.13 and 1559.17 nm, respectively; (c), (d) corresponding pulse-trains; (e), (f) corresponding autocorrelation traces.

wavelength were measured, and the results are presented in Figs. 4(e) and 4(f). As expected, the autocorrelation trace of the harmonic mode-locking soliton has a single peak with pulse duration of 8.37 ps, while three peaks with a separation of 5.16 ps occur on the autocorrelation trace of the bound soliton, which is another typical characteristic of the bound soliton[39,40]. All of these results demonstrated that the dual-wavelength is a composite of two multi-soliton operations, namely the bound soliton and harmonic mode-locking soliton.

It should be noted that the multi-soliton formation is related to the accumulated cavity nonlinear effects experienced by the solitons. Therefore, the composite of different multi-soliton states in our experiments could be attributed to the different cavity nonlinear effects experienced by the two wavelengths. As we know, apart from the bound soliton and harmonic mode-locking soliton, some other multi-soliton operations could also be achieved in fiber lasers, such as soliton rain, soliton liquid, and solitons occupying the whole cavity. However, in our experiments, we only observed these two multi-soliton states and their composite. The reason might be contributed to the limited nonlinear effect provided by the MoS_2-deposited microfiber photonic device, since this photonic device would experience irreversible optical damage when the pump power was increased to higher than 300 mW. Therefore, it is believed that more coexistences of some other multi-soliton operations could be acquired by further improving the performance of the MoS_2-deposited microfiber. On the other hand, it has been demonstrated that graphene and a topological insulator also have saturable absorption and a large nonlinear refractive index[51–53], which indicates that they have the potential to fabricate the microfiber-based photonic device with dual-functions for the investigation of the coexistence of multi-soliton dynamics.

In summary, we experimentally demonstrated the coexistence of a bound soliton and a harmonic mode-locking soliton in an ultrafast fiber laser based on MoS_2-deposited microfiber photonic devices. The bound soliton at 1559.17 nm has the typical spectral modulation with a period of 1.55 nm and pulse separation of 5.16 ps. The harmonic mode-locking soliton at 1555.13 nm has the repetition rate of 479 MHz, corresponding to the 65th harmonic of the fundamental repetition rate. It is believed that the coexistence of multi-soliton states could provide different pulse sources simultaneously for various applications.

This work was partially supported by the National Natural Science Foundation of China (NSFC) (Nos. 61307058, 61378036, 11304101, and 11474108); Guangdong Natural Science Funds for Distinguished Young Scholar (No. 2014A030306019); Program for the Outstanding Innovative Young Talents of Guangdong Province (No. 2014TQ01X220); Program for Outstanding Young Teachers in Guangdong Higher Education Institutes (No. YQ2015051); Science and Technology Project of Guangdong (No. 2016B090925004); Science and Technology Program of Guangzhou (No. 201607010245).

References

1. K. S. Novoselov, D. Jiang, F. Schedin, T. J. Booth, V. V. Khotkevich, S. V. Morozov, and A. K. Geim, PNAS **102**, 10451 (2005).
2. G. Eda and S. A. Maier, ACS Nano **7**, 5660 (2013).
3. S. Z. Butler, S. M. Hollen, L. Cao, Y. Cui, J. A. Gupta, H. R. Gutiérrez, T. F. Heinz, S. S. Hong, J. Huang, A. F. Ismach, E. Johnston-Halperin, M. Kuno, V. V. Plashnitsa, R. D. Robinson,

R. S. Ruoff, S. Salahuddin, J. Shan, L. Shi, M. G. Spencer, M. Terrones, W. Windl, and J. E. Goldberger, ACS Nano **7**, 2898 (2013).
4. Q. L. Bao, H. Zhang, Y. Wang, Z. Ni, Y. Yan, Z. Shen, K. P. Loh, and D. Y. Tang, Adv. Funct. Mater. **19**, 3077 (2009).
5. F. Bonaccorso, Z. Sun, T. Hasan, and A. C. Ferrari, Nat. Photon. **4**, 611 (2010).
6. Z. Sun, T. Hasan, F. Torrisi, D. Popa, G. Privitera, F. Wang, F. Bonaccorso, D. M. Basko, and A. C. Ferrari, ACS Nano **4**, 803 (2010).
7. J. Du, Q. Wang, G. Jiang, C. Xu, C. Zhao, Y. Xiang, Y. Chen, S. Wen, and H. Zhang, Sci. Rep. **4**, 6346 (2014).
8. P. Tang, X. Zhang, C. J. Zhao, Y. Wang, H. Zhang, D. Y. Shen, S. C. Wen, D. Y. Tang, and D. Y. Fan, IEEE Photon. J. **5**, 1500707 (2013).
9. D. Mao, B. Jiang, X. Gan, C. Ma, Y. Chen, C. Zhao, H. Zhang, J. Zheng, and J. Zhao, Photon. Res. **3**, A43 (2015).
10. Y. Chen, G. Jiang, S. Chen, Z. Guo, X. Yu, C. Zhao, H. Zhang, Q. Bao, S. Wen, D. Tang, and D. Fan, Opt. Express **23**, 12823 (2015).
11. S. Lu, Y. Ge, Z. Sun, Z. Huang, R. Cao, C. Zhao, S. Wen, D. Fan, J. Li, and H. Zhang, Photon. Res. **4**, 286 (2016).
12. X. T. Jiang, S. X. Liu, W. Y. Liang, S. J. Luo, Z. L. He, Y. Q. Ge, H. D. Wang, R. Cao, F. Zhang, Q. Wen, J. Q. Li, Q. L. Bao, D. Y. Fan, and H. Zhang, Laser Photon. Rev. 1700229 (2017).
13. L. Lu, Z. M. Liang, L. M. Wu, Y. X. Chen, Y. F. Song, S. C. Dhanabalan, J. S. Ponraj, B. Q. Dong, Y. J. Xiang, F. Xing, D. Y. Fan, and H. Zhang, Laser Photon. Rev. 1700221 (2017).
14. J. N. Coleman, M. Lotya, A. O'Neill, S. D. Bergin, P. J. King, U. Khan, K. Young, A. Gaucher, S. De, R. J. Smith, I. V. Shvets, S. K. Arora, G. Stanton, H. Y. Kim, K. Lee, G. T. Kim, G. S. Duesberg, T. Hallam, J. J. Boland, J. J. Wang, J. F. Donegan, J. C. Grunlan, G. Moriarty, A. Shmeliov, R. J. Nicholls, J. M. Perkins, E. M. Grieveson, K. Theuwissen, D. W. McComb, P. D. Nellist, and V. Nicolosi, Science **331**, 568 (2011).
15. Q. H. Wang, K. Kalantar-Zadeh, A. Kis, J. N. Coleman, and M. S. Strano, Nat. Nanotechnol. **7**, 699 (2012).
16. M. Chhowalla, H. S. Shin, G. Eda, L.-J. Li, K. P. Loh, and H. Zhang, Nat. Chem. **5**, 263 (2013).
17. K. F. Mak, C. Lee, J. Hone, J. Shan, and T. F. Heinz, Phys. Rev. Lett. **105**, 136805 (2010).
18. J. Zheng, H. Zhang, S. Dong, Y. Liu, C. T. Nai, H. S. Shin, H. Y. Jeong, B. Liu, and K. P. Loh, Nat. Commun. **5**, 2995 (2014).
19. K. P. Wang, J. Wang, J. T. Fan, M. Lotya, A. O'Neill, D. Fox, Y. Y. Feng, X. Y. Zhang, B. X. Jiang, Q. Z. Zhao, H. Zhang, J. N. Coleman, L. Zhang, and W. J. Blau, ACS Nano **7**, 9260 (2013).
20. H. Zhang, S. B. Lu, J. Zheng, J. Du, S. C. Wen, D. Y. Tang, and K. P. Loh, Opt. Express **22**, 249 (2014).
21. H. Liu, A. P. Luo, F. Z. Wang, R. Tang, M. Liu, Z. C. Luo, W. C. Xu, C. J. Zhao, and H. Zhang, Opt. Lett. **39**, 4591 (2014).
22. H. Xia, H. Li, C. Lan, C. Li, X. Zhang, S. Zhang, and Y. Liu, Opt. Express **22**, 17341 (2014).
23. Z. Luo, Y. Huang, M. Zhong, Y. Li, J. Wu, B. Xu, H. Xu, Z. Cai, J. Peng, and J. Weng, J. Lightwave Technol. **32**, 4679 (2014).
24. M. Liu, X. W. Zheng, Y. L. Qi, H. Liu, A. P. Luo, Z. C. Luo, W. C. Xu, C. J. Zhao, and H. Zhang, Opt. Express **22**, 22841 (2014).
25. Y. Huang, Z. Q. Luo, Y. Y. Li, M. Zhong, B. Xu, K. J. Che, H. Y. Xu, Z. P. Cai, J. Peng, and J. Weng, Opt. Express **22**, 25258 (2014).
26. R. Khazaeizhad, S. H. Kassani, H. Jeong, D.-I. Yeom, and K. Oh, Opt. Express **22**, 23732 (2014).
27. R. I. Woodward, E. J. R. Kelleher, R. C. T. Howe, G. Hu, F. Torrisi, T. Hasan, S. V. Popov, and J. R. Taylor, Opt. Express **22**, 31113 (2014).
28. M. Zhang, R. C. T. Howe, R. I. Woodward, E. J. R. Kelleher, F. Torrisi, G. H. Hu, S. V. Popov, J. R. Taylor, and T. Hasan, Nano Res. **8**, 1522 (2015).
29. Y. Wang, D. Mao, X. Gan, L. Han, C. Ma, T. Xi, Y. Zhang, W. Shang, S. Hua, and J. Zhao, Opt. Express **23**, 205 (2015).
30. Z. Tian, K. Wu, L. Kong, N. Yang, Y. Wang, R. Chen, W. Hu, J. Xu, and Y. Tang, Laser Phys. Lett. **12**, 065104 (2015).
31. K. Wu, X. Zhang, J. Wang, and J. Chen, Opt. Lett. **40**, 1374 (2015).
32. R. I. Woodward, R. C. T. Howe, G. Hu, F. Torrisi, M. Zhang, T. Hasan, and E. J. R. Kelleher, ACS Appl. Mater. Interfaces **6**, 314 (2014).
33. R. Wang, H. C. Chien, J. Kumar, N. Kumar, H. Y. Chiu, and H. Zhao, ACS Appl. Mater. Interfaces **6**, 314 (2014).
34. J. M. Soto-Crespo and P. Grelu, Lect. Notes Phys. **661**, 207 (2005).
35. A. Haboucha, H. Leblond, M. Salhi, A. Komarov, and F. Sanchez, Phys. Rev. A **78**, 043806 (2008).
36. F. Amrani, A. Haboucha, M. Salhi, H. Leblond, A. Komarov, P. Grelu, and F. Sanchez, Opt. Lett. **34**, 2120 (2009).
37. G. Sobon, J. Sotor, and K. M. Abramski, Appl. Phys. Lett. **100**, 161109 (2012).
38. P. Yan, R. Lin, S. Ruan, A. Liu, and H. Chen, Opt. Express **23**, 154 (2015).
39. D. Y. Tang, W. S. Man, H. Y. Tam, and P. D. Drummond, Phys. Rev. A **64**, 033814 (2001).
40. P. Grelu, F. Belhache, F. Gutty, and J. M. Soto-Crespo, Opt. Lett. **27**, 966 (2002).
41. S. Chouli and P. Grelu, Opt. Express **17**, 11776 (2009).
42. S. Chouli and P. Grelu, Phys. Rev. A **81**, 063829 (2010).
43. M. Horowitz, Y. Barad, and Y. Silberberg, Opt. Lett. **22**, 799 (1997).
44. L. M. Zhao, D. Y. Tang, J. Wu, X. Q. Fu, and S. C. Wen, Opt. Express **15**, 2145 (2007).
45. Y. Q. Huang, Z. A. Hu, H. Cui, Z. C. Luo, A. P. Luo, and W. C. Xu, Opt. Lett. **41**, 4056 (2016).
46. Y. Z. Wang, J. F. Li, E. T. Zhang, K. D. Mo, Y. Y. Wang, F. Liu, X. J. Zhou, and Y. Liu, Opt. Lett. **38**, 5212 (2013).
47. Z. C. Luo, M. Liu, H. Liu, X. W. Zheng, A. P. Luo, C. J. Zhao, H. Zhang, S. C. Wen, and W. C. Xu, Opt. Lett. **38**, 5212 (2013).
48. A. P. Luo, M. Liu, X. D. Wang, Q. Y. Ning, W. C. Xu, and Z. C. Luo, Photon. Res. **3**, A69 (2015).
49. L. E. Nelson, D. J. Jones, K. Tamura, H. A. Haus, and E. P. Ippen, Appl. Phys. B **65**, 277 (1997).
50. H. Zhang, D. Y. Tang, X. Wu, and L. M. Zhao, Opt. Express **17**, 12692 (2009).
51. H. Zhang, S. Virally, Q. Bao, L. K. Ping, S. Massar, N. Godbout, and P. Kockaert, Opt. Lett. **37**, 1856 (2012).
52. S. Lu, C. Zhao, Y. Zou, S. Chen, Y. Chen, Y. Li, H. Zhang, S. Wen, and D. Tang, Opt. Express **21**, 2072 (2013).
53. W. J. Liu, L. Pang, H. Han, W. Tian, H. Chen, M. Lei, P. G. Yan, and Z. Wei, Sci. Rep. **6**, 19997 (2016).